Topography correlated atmospheric delay correction in radar interferometry using wavelet transforms

M. Shirzaei[1] and R. Bürgmann[1]

Received 11 October 2011; revised 26 November 2011; accepted 30 November 2011; published 6 January 2012.

[1] Atmospheric delay is one of the major sources of error in repeat pass interferometry. We propose a new approach for correcting the topography-correlated components of this artifact. To this aim we use multiresolution wavelet analysis to identify the components of the unwrapped interferogram that correlate with topography. By using a forward wavelet transform we break down the digital elevation model and the unwrapped interferogram into their building blocks based on their frequency properties. We apply a cross-correlation analysis to identify correlated coefficients that represent the effect of the atmospheric delay. Thus, the correction to the unwrapped interferogram is obtained by down-weighting the correlated coefficients during inverse wavelet transform. We test this approach on real and synthetic data sets that are generated over the San Francisco Bay Area. We find that even in the presence of tectonic signals, this method is able to reduce the correlated component of the atmospheric delay by up to 75% and improves the signal in areas of high relief. The remaining part is most likely due to 3D heterogeneities of the atmosphere and can be reduced by integrating temporal information or using complementary observations or models of atmospheric delay. **Citation:** Shirzaei, M., and R. Bürgmann (2012), Topography correlated atmospheric delay correction in radar interferometry using wavelet transforms, *Geophys. Res. Lett.*, *39*, L01305, doi:10.1029/2011GL049971.

1. Introduction

[2] Differential interferometric synthetic aperture radar (InSAR) provides high resolution observations of ground surface motion [*Bürgmann et al.*, 2000; *Hanssen*, 2001]. The procedure of InSAR involves interfering two overlapping SAR images acquired from similar viewing geometry and subtracting geometrical phase contributions using satellite ephemeris data and a reference Digital Elevation Model (DEM) [*Ferretti et al.*, 2007]. The observed interferometric phase in each interferogram mostly contains contributions from ground displacement, DEM inaccuracy, atmospheric delay, and satellite state vector errors [*Ferretti et al.*, 2007].

[3] In particular, atmospheric delay often imposes significant artifacts in radar data and comprises three major components; wet, hydrostatic and ionospheric, which are induced by variation in refractivity index of the atmosphere due to dipole components of troposphere water vapor, pressure to temperature ratio changes of the troposphere and spatiotemporal variations in ionospheric electron density, respectively [*Lin et al.*, 2010]. The effect of atmospheric delay consists of two parts [*Hanssen*, 2001]; 1) the effect of 3D heterogeneities of the atmosphere, which similarly affects plains and mountains, and 2) vertical stratification of the atmosphere that causes height-dependent refractivity variations. The first component is mostly topography independent and varies gradually over an area, can be characterized as a second-order stationary process and is well parameterized using fractal statistics [*Hanssen*, 2001]. The second component correlates with topography and may vary as a linear function of the altitude, therefore, a model assuming a linear relation between deformation and topography can be used to correct it [e.g., *Cavalie et al.*, 2007].

[4] Correcting the topography correlated atmospheric delay (TCAD) is not a trivial task as it may correlate in time and has a variable spatial pattern related to the surface topography. Moreover, this effect depends on the scale of local relief; it may be non-linear function of elevation and may vary across an area. Several methods have already been suggested to correct TCAD, which require external data or redundant observation and/or deal only with the linearly correlated atmospheric delay [e.g., *Cavalie et al.*, 2007; *Doin et al.*, 2009; *Jolivet et al.*, 2011; *Lin et al.*, 2010]. Here, we propose and test a new approach to correct TCAD that employs wavelet transforms. In this method we use wavelet multiresolution analysis [*Mallat*, 1989] to decompose the InSAR range-change map and DEM into their building blocks based on different spatial scales. Then by cross correlating their associated wavelet coefficients, we identify the common coefficients of the DEM and InSAR data. The correction is obtained by down-weighting the wavelet coefficients with high correlation values during inverse wavelet analysis. In the following sections we describe the details of our method and validate it on real and synthetic data sets.

2. Methods

2.1. Wavelet Multiresolution Analysis

[5] Multiresolution analysis decomposes a signal into its building blocks according to their frequency properties [*Mallat*, 1989]. Assuming $\Theta(\zeta,\eta)$ to be a 2D image (e.g., unwrapped interferogram) with a size of $p \times q$, it can be decomposed in the wavelet domain by using a multiresolution analysis [*Mallat*, 1989] as follows:

$$\Theta(\zeta,\eta) = \sum_{i_x}^{p-1}\sum_{i_y}^{q-1} v_{i_x i_y}\Phi_{J i_x i_y}(\zeta,\eta) + \sum_{j'}^{J-1}\sum_{i_x}^{p-1}\sum_{i_y}^{q-1}\sum_{\varepsilon}^{3} w^{\varepsilon}_{j' i_x i_y}\Psi^{\varepsilon}_{j' i_x i_y}(\zeta,\eta) \quad (1)$$

[1]Department of Earth and Planetary Science, University of California, Berkeley, California, USA.

$$\Psi^{\varepsilon}_{j'i_x i_y}(\zeta,\eta) = \begin{cases} \Psi^{\varepsilon}_{j'i_x}(\zeta).\Phi^{\varepsilon}_{j'i_y}(\eta), & \varepsilon = 1 \\ \Phi^{\varepsilon}_{j'i_x}(\zeta).\Psi^{\varepsilon}_{j'i_y}(\eta), & \varepsilon = 2 \\ \Psi^{\varepsilon}_{j'i_x}(\zeta).\Psi^{\varepsilon}_{j'i_y}(\eta), & \varepsilon = 3 \end{cases}$$

$$\Phi_{Ji_x i_y}(\zeta,\eta) = \Phi_{Ji_x}(\zeta).\Phi_{Ji_y}(\eta)$$

and

$$w^{\varepsilon}_{j'i_x i_y} = \left\langle \Theta(\zeta,\eta), \Psi^{\varepsilon}_{j'i_x i_y}(\zeta,\eta) \right\rangle \quad , \quad v_{j'i_x i_y} = \left\langle \Theta(\zeta,\eta), \Phi_{j'i_x i_y}(\zeta,\eta) \right\rangle \tag{2}$$

where Φ and Ψ are the smoothing and the mother wavelet functions, respectively, v and w are the associated smoothing and wavelet coefficients, J is the number of wavelet scales, and $\langle .,. \rangle$ is the inner product operator.

[6] The number of scales for wavelet decomposition is specified such that the effective wavelet window size is roughly the spatial extent of the TCAD. This wavelength might be estimated either visually or based on a priori information. The effective window size is twice the root mean square radius (*rmsr*) of the wavelet function, which is calculated using the following equation [*Goswami and Chan*, 1999]:

$$rmsr = \frac{1}{\|\Psi\|}\left[\int_{-\infty}^{+\infty}(x-x^*)^2|\Psi(x)|^2dx\right]^{1/2} \quad , \quad x = \xi,\eta \tag{3}$$

$$x^* = \frac{1}{\|\Psi\|^2}\int_{-\infty}^{+\infty} x|\Psi(x)|^2dx$$

$$\|\Psi\| = \left[\int_{-\infty}^{+\infty}|\Psi(x)|^2dx\right]^{1/2}$$

where $|.|$ is the absolute value operator. Here, it is assumed that *rmsr* is a square in both coordinate dimensions.

2.2. Correcting the Topography-Correlated Atmospheric Delay

[7] Assuming $U(\zeta,\eta)$ and $D(\zeta,\eta)$ are the unwrapped interferogram and DEM registered to the interferogram in the radar coordinate system, following equation (1) the associated wavelet multiresolution analyses are

$$\begin{aligned} U(\zeta,\eta) = &\sum_{i_x}^{p-1}\sum_{i_y}^{q-1} {}^{u}v_{i_x i_y}\Phi_{Ji_x i_y}(\zeta,\eta) \\ &+ \sum_{j'}^{J-1}\sum_{i_x}^{p-1}\sum_{i_y}^{q-1}\sum_{\varepsilon}^{3} {}^{u}w^{\varepsilon}_{j'i_x i_y}\Psi^{\varepsilon}_{j'i_x i_y}(\zeta,\eta) \end{aligned} \tag{4}$$

$$\begin{aligned} D(\zeta,\eta) = &\sum_{i_x}^{p-1}\sum_{i_y}^{q-1} {}^{d}v_{i_x i_y}\Phi_{Ji_x i_y}(\zeta,\eta) \\ &+ \sum_{j'}^{J-1}\sum_{i_x}^{p-1}\sum_{i_y}^{q-1}\sum_{\varepsilon}^{3} {}^{d}w^{\varepsilon}_{j'i_x i_y}\Psi^{\varepsilon}_{j'i_x i_y}(\zeta,\eta) \end{aligned}$$

where, ${}^{u}w$ and ${}^{d}w$ are high frequency coefficients of the unwrapped interferogram and DEM, respectively, and are obtained using equation (2). If the range-change map contains a component similar to the topography such as from TCAD, some of the high frequency components of the unwrapped interferogram correlate with the equivalent coefficients of the DEM; i.e., some of their wavelet coefficients are found to have similar values. To evaluate this similarity we calculate the cross-correlation matrix of the wavelet coefficients for each scale (j') as follows;

$$C^{\varepsilon}_{j'} = {}^{u}w^{\varepsilon}_{j'} \circ {}^{d}w^{\varepsilon}_{j'} \tag{5}$$

where, $\circ$ is the operator of matrix correlation. Following the identification of the correlated coefficients, one way to reduce their effect is to set them to zero. However, a more sophisticated approach is to down-weight them according to their correlation value. The equivalent down-weighted wavelet coefficients of the unwrapped interferogram can be obtained as follows;

$${}^{u}\widehat{w}^{\varepsilon}_{j'} = \left(1 - C^{\varepsilon}_{j'}\right){}^{u}w^{\varepsilon}_{j'} \tag{6}$$

where ${}^{u}\widehat{w}^{\varepsilon}_{j'}$ provides the corrected coefficients, which will be zero if the associated correlation coefficient is 1. Following down-weighting the correlated coefficients, the corrected unwrapped interferogram can be obtained by evaluating equation (1) using the new coefficients.

[9] This approach for correcting TCAD can also be applied to wrapped interferograms. In this case, the real and imaginary part of the interferometric phase should be corrected separately. This becomes important when, due to low phase coherence, proper phase unwrapping is not possible. However, phase discontinuities due to unwrapping error should not affect the result obtained by our approach, because they are not correlated with the DEM.

3. Validation Test

3.1. One-Day Interferogram

[10] To demonstrate the validity of our approach we apply it to a 1-day interferogram generated by from SAR images acquired in descending orbit mode of the ERS-1 and ERS-2 satellites (Track 70, Frame 2853) over the San Francisco Bay Area (Figure 1a). The master and slave images of this interferogram were acquired on 1996/03/29 and 1996/03/30, therefore, one can assume that no surface motion is measured and the phase change is mostly due to atmospheric delay. SRTM DEM and Delft precise orbits are used to flatten the interferogram. The interferogram is multilooked by factors of 4 and 20 along range and azimuth, which yields a pixel size of $\sim$80 $\times$ 80 m^2. Figures 1b–1e show the interferogram, the associated coherence map, the unwrapped interferogram, and DEM in radar coordinate system, respectively. The unwrapped interferogram is obtained by applying a minimum cost flow approach [*Chen and Zebker*, 2001] to those pixels that present coherence above 0.3 [*Costantini and Rosen*, 1999]. In Figure 1d we marked an area of significant phase change (Label A) that corresponds to an area of high relief in the California Coast Ranges. We also note a longer-wavelength feature on the western (oceanward) flank of the Santa Cruz Mountains south of San Francisco (Label B),

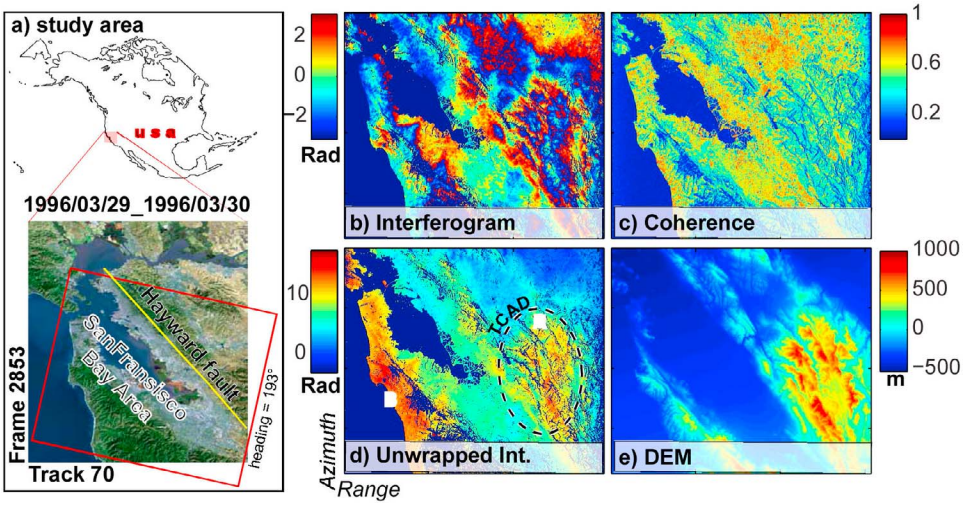

Figure 1. (a) Study area and the foot print of the ERS SAR scenes used for interferometry. (b) Differential 1-day interferogram used in this study. (c) Interferometric coherence map. (d) Unwrapped interferogram, the location of strongly topography correlated signal is marked. (e) SRTM DEM transferred to the radar coordinate system. In Figure 1d, the pixels with coherence below 0.3 are masked out. Although a residual orbital ramp is evident in Figure 1d, we did not attempt to correct it. In Figure 1d, TCAD = topography correlated atmospheric delay.

which we suspect to be an artifact associated with coastal fog or troposphere that also correlates with topography. The linear cross correlation between the unwrapped interferogram and the DEM is ∼42% (see also Figure S1 in the auxiliary material), suggesting that a large part of the observed phase change is due to TCAD.[1]

[11] To begin the algorithm we need to choose an appropriate wavelet function. This choice should provide a balance between computation and spectral resolution, which determines the ability of the wavelet function to distinguish between different frequency components. Continuous wavelet transforms (CWT) provide a very fine resolution at the expense of computation time [*Goswami and Chan*, 1999]. Wavelet packets have lower resolution but are more efficient to compute compared with CWT [*Goswami and Chan*, 1999]. Discrete wavelet transforms (DWT) also have relatively low resolution but there are very efficient algorithms to compute forward and inverse transforms. In our exercise we start with the simplest but fastest class, the DWT.

[12] The correlation between the corrected interferogram and DEM is the criterion for the effectiveness of the chosen wavelet function. Accordingly, the most suitable wavelet family is the one that reduces this correlation significantly. The first investigated DWT wavelet function is the near symmetric wavelet family *Coiflet* of order N ($N = 5$), which has a support width of $6N - 1$ and number of vanishing moments of $2N$ [*Daubechies*, 1992]. Assuming the correlated component of the atmospheric delay to have a variety of wavelengths from pixel size to broader scales as large as the whole interferogram, we choose the number of scales for the wavelet decomposition. This task is accomplished by using equation (3), which relates the wavelet scale to the effective window size. As a result we find that the wavelet with scales ranging from 1 to 10 provides an effective window size from ∼80 m to ∼80 km.

[13] For evaluating the wavelet transform, the data should be continuous on a regular grid. Therefore, we filled the gaps associated with low-coherence pixels by using a linear interpolation. In the following, the wavelet decomposition of the unwrapped interferogram and DEM is obtained using equation (2). Figure 2a presents the wavelet coefficients of the decomposed unwrapped interferogram for 10 scales. Then, we calculate the cross correlation between coefficients of the DEM and the unwrapped interferogram for each level of decomposition and down-weight the correlated ones using equation (6). The updated wavelet coefficients are shown in Figure 2b. In the next step, the corrected unwrapped interferogram is obtained by computing the inverse wavelet transform (equation (1)) using the corrected coefficients.

[14] The corrected interferogram and the estimated TCAD are presented in Figures 3a and 3b, respectively. Clearly, most of the correlated parts of the signal are removed. The linear correlation between the corrected interferogram and DEM is ∼12% which represents a reduction of 75% from the original interferogram. Application of other DWT functions such as the Daubechies family [*Daubechies*, 1992] gives similar results. Since the correction obtained by using discrete wavelets is quite effective we did not try to use continuous or packet wavelets.

[15] This test demonstrates the ability of our method to correct TCAD for the case that no surface motion is present in the interferogram. In the next section we test the strength of our method in the presence of a tectonic signal that contributes an additional component to our interferogram.

3.2. Ten-Year Interferogram

[16] To simulate an interferogram that spans 10 years of tectonic deformation in the region, we superimpose the 1-day interferogram with synthetic displacements due to aseismic slip on the Hayward fault (Figures 4a and 4b) and regional plate boundary deformation (Figure 4c) for 10 years. To this aim we use the creep model proposed for the Hayward fault (Figure 4a) following earlier works [*Schmidt et al.*, 2005] and

[1]Auxiliary materials are available in the HTML. doi:10.1029/2011GL049971.

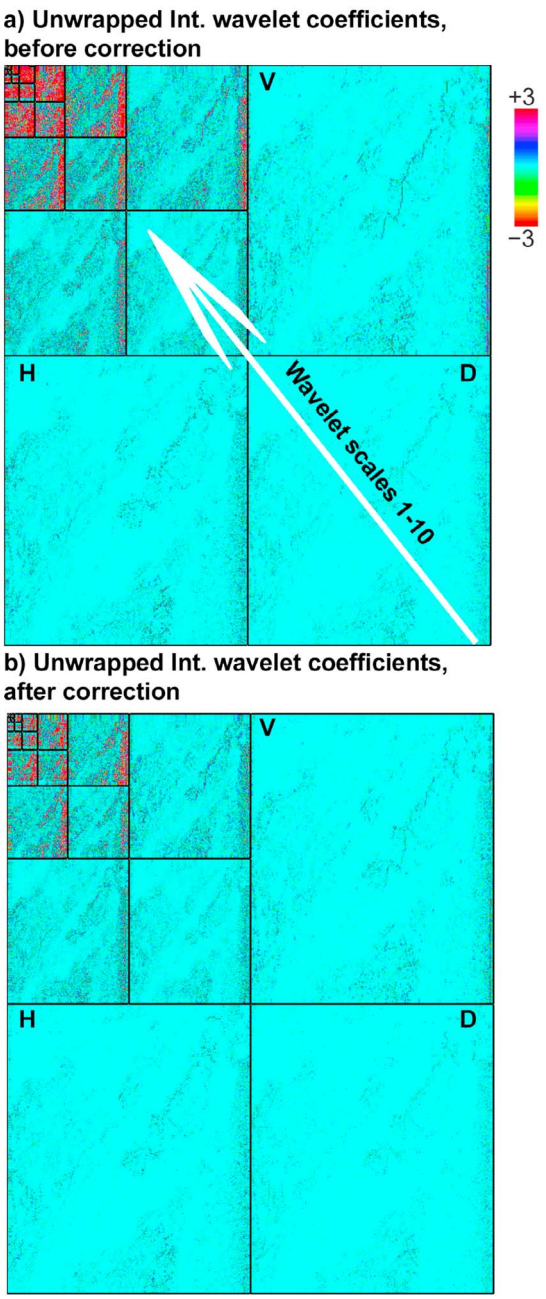

Figure 2. The associated coefficients of 10 level wavelet decomposition of the unwrapped interferogram using Coiflet family. (a, b) Before and after correction for atmospheric delay, respectively. (D: $\varepsilon = 1$, V: $\varepsilon = 2$, H: $\varepsilon = 3$ in equation (1).)

a buried dislocation source extending below the Hayward fault (12 km depth) SE with a slip rate of 40 mm/yr [*Argus and Gordon*, 2001]. These model components are obtained from joint inversion of InSAR, GPS, creepmeter, and seismic data and represent the annual aseismic creep of the Hayward fault and the regional strain associated with the transform plate boundary of the San Andreas Fault system, respectively. The synthetic displacement is obtained through a forward calculation that associates the slip at depth to the displacement at the surface through dislocation theory [see, e.g., *Okada*, 1985]. The model shown in Figure 4a presents

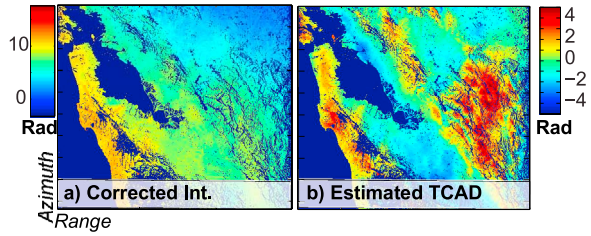

Figure 3. (a) One-day interferogram corrected for topography correlated atmospheric delay. (b) The estimated TCAD (topography-correlated atmospheric delay). No attempt was made to re-estimate orbits. This doesn't affect the wavelet analysis, while it could impact the result of methods using only linear correlation.

the Hayward-fault slip rates and to generate the 10-year slip model we multiply the slip values by a factor of 10, assuming steady rates. The obtained surface displacements after projection to the radar coordinate system are shown in Figures 4b and 4c. Adding these displacements to the unwrapped interferogram of the 1-day image pair yields a 10-year synthetic interferogram as shown in Figure 4d.

[17] By applying the same procedure as explained for the 1-day interferogram, we obtain the corrected TCAD for the synthetic 10-year interferogram (Figure 4e). Comparing Figures 3b and 4e we find that despite inclusion of the tectonic signal the corrected TCAD are identical. The mean and standard deviation of the difference between these two

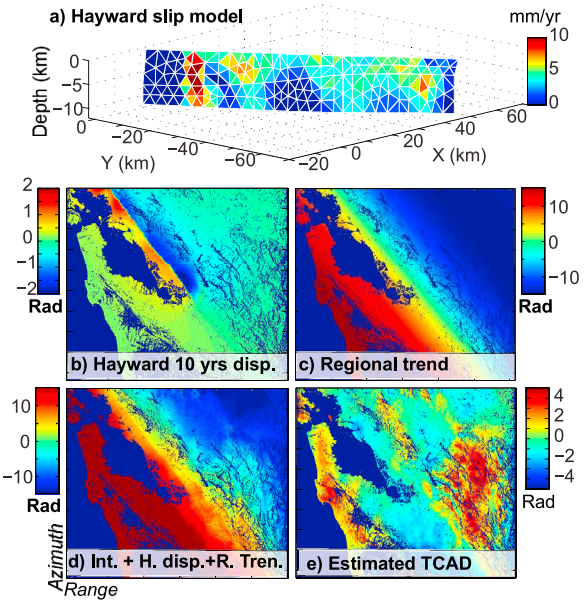

Figure 4. (a) Distributed slip model proposed for Hayward fault showing average aseismic slip rates inverted from surface deformation and seismicity-rate data [*Schmidt et al.*, 2005]. (b, c) Simulated surface displacement from 10 years of aseismic slip on the Hayward fault (from Figure 4a) and a first order model of the regional strain associated with the San Andreas Fault system, respectively. (d) Synthetic unwrapped interferogram as a result of superimposition of the Figures 4b, 4c, and 1d. (e) The estimated TCAD (topography-correlated atmospheric delay).

corrections are 0.04 rad and 0.3 rad, respectively, equivalent to 0.2 mm and 1.4 mm LOS displacement. This negligible difference shows the success of the proposed method in extracting the atmospheric delay even in the presence of a large and broad scale signal of ground motion.

4. Discussion

[18] We presented a new algorithm for correcting topography-correlated atmospheric delay by using wavelet multiresolution analysis. Wavelet transforms decompose signals into building blocks based on a variety of spatial/temporal scales. The reason we chose wavelets lies in their fine spectral resolution and the availability of methods to evaluate wavelets in near real time manner [*Goswami and Chan*, 1999]. For two correlated signals that contain components with similar frequency properties, the obtained wavelet coefficients have similar values over a range of scales, which represents the key rationale for our approach. Following decomposition of both the unwrapped interferogram and DEM in the wavelet domain, the correlated coefficients of the interferogram and DEM are most likely to be a result of TCAD. In most applications of the wavelet transforms, the choice of wavelet family is critical. However, in our study this choice is rather straightforward. We choose a wavelet that reduces the correlation between the corrected unwrapped interferogram and DEM. This can be done in an optimization manner; i.e., large families of different wavelets are implemented and an ensemble of the corrected interferograms is produced. The optimum wavelet family is the one that yields the minimum correlation between the corrected unwrapped interferogram and the DEM. We find that among the tested DWT families, the Coiflet order of 5 has this advantage while being efficient to evaluate. One should note that continuous wavelets and wavelet packets would certainly perform as well as the Coiflet wavelet family, but at the expense of computation time.

[19] The main assumption of the presented algorithm here is that the tectonic signal is not correlated with topography. This is likely to be a valid assumption for the strike-slip faulting we consider; however, in the case of deformation due to magma chamber inflation below active volcanoes [e.g., *Bathke et al.*, 2011] or when studying actively growing fold and thrust systems, short-term surface displacement may be strongly correlated with topography. In such cases, this approach for correcting TCAD should be applied with caution. This is due to the fact that in these environments the frequency and statistical characteristics of the ground surface displacement and TCAD in broader wavelet scales can be very similar. This may cause overcorrection of the long wavelength of the ground displacement. However, this method is still applicable following careful tuning of the wavelet scales corresponding to different spatial scales of the TCAD. For instance, instead of applying the correction to all wavelet scales, we can use only those that have effective window length different than the extent of main geological features such as faults or volcanic calderas. Moreover, introducing thresholds for the maximum amplitude of the TCAD can also be useful when weighting the wavelet coefficients. However, the information required to threshold wavelet coefficients may not be available everywhere.

[20] We applied our method to an unwrapped interferogram; however, this approach is applicable to wrapped interferograms as well. To this aim the real and imaginary part of the complex interferometric phase should be corrected separately.

[21] This approach for correcting TCAD can be successfully implemented in multitemporal InSAR algorithms as it is very efficient to evaluate for each individual interferogram. Moreover, it does not affect other components of the interferogram such as surface motion due to tectonic and volcanic activities.

5. Conclusion

[22] A new method for correcting the topography-correlated atmospheric delay in repeat pass interferometry is presented. This method uses wavelet multiresolution analysis and identifies the topography-correlated components of the unwrapped interferogram as an atmospheric delay. We successfully tested this method on a 1-day interferogram and a 10-year synthetic interferogram over the San Francisco Bay Area. Both real and simulated examples demonstrate the success of the presented method for correcting for the topography-correlated component of the atmospheric delay, even in the presence of a strong deformation signal. This method does not require redundant observations and can be efficiently applied to individual interferograms. Moreover, in this method we do not need to remove the effect of other contributions to LOS displacement such as ground motion or residual orbital error.

[23] **Acknowledgments.** We would like to thank the WInSAR archive at UNAVCO for supplying ERS images. The interferogram used in this study was generated using the GMTSAR software [*Sandwell et al.*, 2011].

[24] The Editor thanks two anonymous reviewers for their assistance in evaluating this paper.

References

Argus, D. F., and R. G. Gordon (2001), Present tectonic motion across the Coast Ranges and San Andreas fault system in central California, *Geol. Soc. Am. Bull.*, *113*(12), 1580–1592, doi:10.1130/0016-7606(2001)113<1580:PTMATC>2.0.CO;2.

Bathke, H., M. Shirzaei, and T. R. Walter (2011), Inflation and deflation at the steep-sided Llaima stratovolcano (Chile) detected by using InSAR, *Geophys. Res. Lett.*, *38*, L10304, doi:10.1029/2011GL047168.

Bürgmann, R., P. A. Rosen, and E. J. Fielding (2000), Synthetic aperture radar interferometry to measure Earth's surface topography and its deformation, *Annu. Rev. Earth Planet. Sci.*, *28*, 169–209, doi:10.1146/annurev.earth.28.1.169.

Cavalie, O., M. P. Doin, C. Lasserre, and P. Briole (2007), Ground motion measurement in the Lake Mead area, Nevada, by differential synthetic aperture radar interferometry time series analysis: Probing the lithosphere rheological structure, *J. Geophys. Res.*, *112*, B03403, doi:10.1029/2006JB004344.

Chen, C. W., and H. A. Zebker (2001), Two-dimensional phase unwrapping with use of statistical models for cost functions in nonlinear optimization, *J. Opt. Soc. Am. A Opt. Image Sci. Vis.*, *18*, 338–351, doi:10.1364/JOSAA.18.000338.

Costantini, M., and P. A. Rosen (1999), A generalized phase unwrapping approach for sparse data, paper presented at the 1999 International Geoscience and Remote Sensing Symposium (IGARSS), Inst. of Electr. and Electron. Eng., Hamburg, Germany.

Daubechies, I. (1992), *Ten Lectures on Wavelets*, 377 pp., Soc. for Ind. and Appl. Math., Philadelphia, Pa.

Doin, M. P., C. Lasserre, G. Peltzer, O. Cavalie, and C. Doubre (2009), Corrections of stratified tropospheric delays in SAR interferometry: Validation with global atmospheric models, *J. Appl. Geophys.*, *69*(1), 35–50, doi:10.1016/j.jappgeo.2009.03.010.

Ferretti, A., A. Monti-Guarnieri, C. Prati, F. Rocca, and D. Massonnet (Eds.) (2007), *InSAR Principles: Guidelines for SAR Interferometry Processing and Interpretation*, *Eur. Space Agency Tech. Memo.*, *19*, 48 pp.

Goswami, J. C., and A. K. Chan (1999), *Fundamentals of Wavelets: Theory, Algorithms, and Applications*, 324 pp., Wiley-Intersci., New York.

Hanssen, R. F. (2001), *Radar Interferometry, Data Interpretation and Error Analysis*, 328 pp., Kluwer Acad., Dordrecht, Netherlands.

Jolivet, R., R. Grandin, C. Lasserre, M.-P. Doin, and G. Peltzer (2011), Systematic InSAR tropospheric phase delay corrections from global meteorological reanalysis data, *Geophys. Res. Lett.*, *38*, L17311, doi:10.1029/2011GL048757.

Lin, Y. N., M. Simons, E. A. Hetland, P. Muse, and C. DiCaprio (2010), A multiscale approach to estimating topographically correlated propagation delays in radar interferograms, *Geochem. Geophys. Geosyst.*, *11*, Q09002, doi:10.1029/2010GC003228.

Mallat, S. G. (1989), A theory for multiresolution signal decomposition: The wavelet representation, *IEEE Trans. Pattern Anal. Mach. Intell.*, *11*(7), 674–693, doi:10.1109/34.192463.

Okada, Y. (1985), Surface deformation due to shear and tensile faults in a half-space, *Bull. Seism. Soc. Am.*, *75*, 1135–1154.

Sandwell, D., R. Mellors, X. Tong, M. Wei, and P. Wessel (2011), Open radar interferometry software for mapping surface deformation, *Eos Trans. AGU*, *92*(28), 234 doi:10.1029/2011EO280002.

Schmidt, D. A., R. Bürgmann, R. M. Nadeau, and M. d'Alessio (2005), Distribution of aseismic slip rate on the Hayward fault inferred from seismic and geodetic data, *J. Geophys. Res.*, *110*, B08406, doi:10.1029/2004JB003397.

R. Bürgmann and M. Shirzaei, Department of Earth and Planetary Science, University of California, Berkeley, CA 94720, USA. (shirzaei@berkeley.edu)